Improved GPR Image Quality by Truncating the Bandwidth of the Fourier Transform in 2D Diffraction Tomographic Inversion

Sebastian HerHuat Lum, Tee Tang and Jim Lyall

Faculty of Built Environment and Engineering,
Queensland University of Technology, Brisbane, Australia.
hh.lum@student.qut.edu.au, t.tang@qut.edu.au, j.lyall@qut.edu.au.

Abstract – Diffraction tomography (DT) has been applied in ground penetrating radar (GPR) to obtain images of buried objects. In order to obtain a unique solution for the object function, a maximum frequency range should be used in a DT inversion routine. In this paper, a method is proposed to appropriately truncate the frequency range of the Fourier-transformed (FT) scattered field for a 2D DT inversion routine. This is achieved by determining the variation of the phase in the FT scattered field. The number of zero-crossings of the FT phase along the spatial axis is counted and a moving-average filter is applied to enable proper bandwidth selection. Numerical simulations are demonstrated using synthetic data with additive white Gaussian noise.

Keywords: Diffraction tomography; Fourier Transform; ground penetrating radar

1. Introduction

Ground penetrating radar (GPR) adopts the ultra-wideband antenna technology to transmit high frequency electromagnetic pulses into the ground and to receive the reflected waves scattered by buried objects [1]. With the diffraction tomographic (DT) inversion technique, the captured GPR data can then be manipulated and processed to illustrate the cross-sectional image of the test ground. This non-destructive technique is able to detect, locate and identify buried objects without the need of ground digging or excavation. As a result, GPR has found a wide variety of applications in forensic investigation, archaeology surveying, landmine detection, geophysical probing and through-wall imaging [2-4].

DT inversion shows a linear relation between the spatial Fourier transform of the object function and the scattered field [5]. The principle of diffraction tomography is based on the first order Born approximation which assumes that the buried object of interest is a weak scatterer. A few additional assumptions are also invoked during the process of DT derivation to simplify and linearize the nonlinear electric field integral equation. These assumptions have incurred a trade-off to the reconstruction of the buried objects especially for the practical usage when noise is present in the collected field data. Noise can be caused by uneven ground surface and inhomogeneities in the test ground.

In recent years, researchers have significantly improved the image quality of reconstructed buried objects. For instance, Hansen and Johansen introduced a DT algorithm that takes air-soil interface into consideration for a lossless background [6]. Cui and Chew proposed an inversion scheme that takes account of the electrical conductivity of lossy soil [7]. Furthermore, Hislop and Tang developed an inversion routine that is able to avoid the asymptotic formulation and to overcome the evanescent waves for shallowly buried objects [8].

However, attention must also be given to the bandwidth selection when performing the DT inversion computation. In the spatial-frequency domain, a single-frequency scattered field data corresponds to samples of the object function along a semicircular arc, when a lossless ground is assumed [9]. The electrical parameters of the buried object relative to the background soil are termed as the object function. In order to get a unique solution for the object function, one must attempt to fill in all the information on the spatial-frequency domain. Since GPR has limited scanning angles (instead of 360˚ around the measurement domain), a frequency range from 0 to ∞ is preferred to overcome the physical measurement limitation. It is common in practice that the frequency range truncation for the inversion calculation is determined from the magnitude spectrum of the FT scattered field [5-8]. This is because after a certain frequency the magnitude spectrum of the FT scattered field is almost zero. As a result, a maximum threshold frequency is chosen for bandwidth truncation.

In this paper, we propose an alternative bandwidth truncation method to select the frequency range for a 2D bistatic GPR inversion algorithm through the phase variation of the FT scattered field data. We count the number of zero-crossings of the phase along the spatial axis of each frequency. A moving average of the zero-crossing count over the frequencies is generated and a threshold is used to determine the bandwidth truncation.

2. Moving Average Zero-Crossing Count

A fixed-offset bistatic GPR configuration, as shown in Figure 1, is used to illustrate the proposed moving average zero-crossing count method. A planar interface (z = 0) separates the test model into air and ground. The transmitting and receiving antennas are assumed to be ideal Hertzian dipoles and they move over a length of 1.44 m in 2 cm steps along y-axis. The ground permittivity ε_g is $4\varepsilon_0$ and the object permittivity ε_ρ is $8\varepsilon_0$. The ground conductivity σ_g and the object conductivity σ_ρ are 10 mS/m. A Gaussian excitation current with a centre frequency f_c of 300 MHz is applied to the transmitting antenna. The synthetic time-domain scattered field data is generated using the GPRMax simulation tool [10].

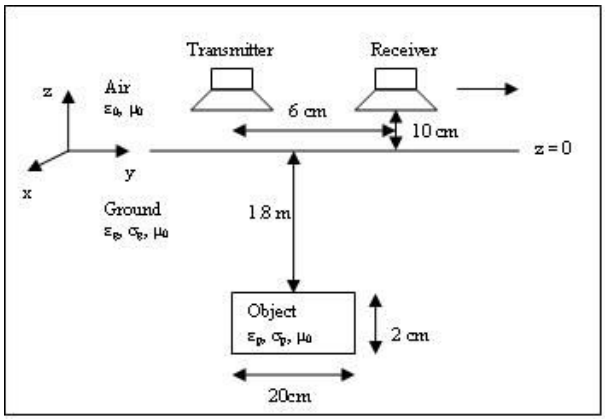

Figure 1: A fixed-offset bistatic GPR configuration.

The 2D FT of the time-domain scattered field can be seen in Figure 2. From the magnitude spectrum of Figure 2(a), we noticed the spectrum gives indication to frequencies with magnitude close to zero. One may choose the frequency range visually from 60 MHz to 800 MHz. On the other hand, we can select the bandwidth visually from 21 MHz (the lowest frequency point) to 1.3 GHz from the variation of the phase spectrum of Figure 2(b). With this broader bandwidth, several DT inversion algorithms have been shown to provide good image quality. However, the reconstructed images start to distort if frequencies higher than 1.3 GHz is selected. It is obvious that it is not easy to visually determine the correct threshold frequency from the spectral phase plot of Figure 2(b).

In order to establish a methodological process to determine the minimum and maximum frequencies, we first examine the characteristics of the spatial phase variation at each frequency. To illustrate the principle, the spatial phase variations at four selected frequencies are shown in Figure 3. In the figure, the phase tends to evolve around the centre of the spatial axis and spread out. The phase at 1.8 GHz (Figure 3(d)) appears to have irregular "noise-like" variations over the entire spatial axis. However, when one looks carefully, there are more phase oscillations at the zero-phase boundary than that of the other three lower frequencies. In addition, we also observed that in the lower two frequencies, i.e., 636 MHz and 975 MHz (Figure 3(a)-(b)), there are only a small number of zero crossings. With this knowledge, we conclude that counting the zero-crossings can be an effective way to detect the workable frequency range.

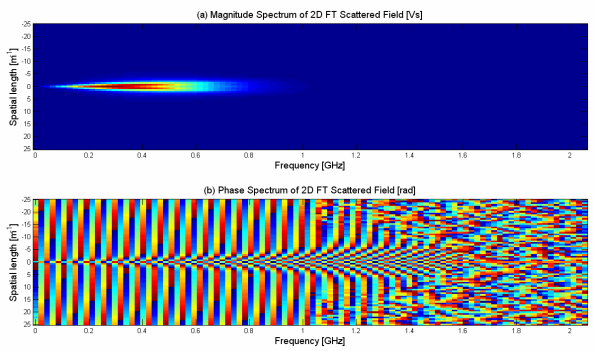

Figure 2: The 2D FT scattered field in the spatial-frequency domain with frequency step of 21 MHz. (a) Magnitude spectrum. (b) Phase spectrum.

A zero-crossing count (ZCC) is incremented for each positive-crossing and negative-crossing phase value. It is applied to each frequency, as illustrated in Figure 4. A moving average filter (MA) is used and the window size of the MA filter is determined from the average value of the rate of change of the ZCC. The average value of the ZCC is taken as a threshold to determine the minimum and maximum frequencies. The minimum frequency is defined as: (a) the lowest (first) frequency if there is no crossing between 0 and f_c; (b) the $\frac{1}{2}f_c$ if there is no crossing between 0 and $\frac{1}{2}f_c$ but there is crossing between $\frac{1}{2}f_c$ and f_c; or (c) the last highest positive or negative crossing frequency up to and including $\frac{1}{2}f_c$ if there is crossing between 0 and $\frac{1}{2}f_c$ only. Note: if there are crossing betweens 0 and $\frac{1}{2}f_c$ as well as between $\frac{1}{2}f_c$ and f_c, the inversion image cannot be meaningfully reconstructed because this represents a noisy dataset. The maximum frequency is defined as: either (a) the positive-crossing frequency if there is only one positive crossing between the minimum frequency and $4f_c$; or (b) the last positive-crossing frequency if there are multiple positive crossings between minimum frequency and $4f_c$, and the frequency samples between the last positive crossing and the preceding negative crossing are at least twice the moving average window size.

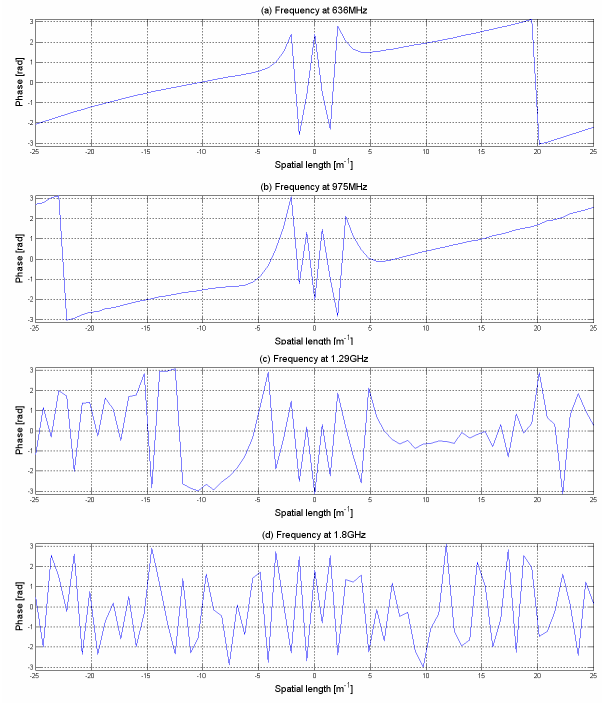

Figure 3: Phase plot against the spatial axis at four different frequencies which are (a) 636 MHz, (b) 975 MHz, (c) 1.29 GHz and (d) 1.8 GHz from the phase spectrum of the 2D FT scattered field.

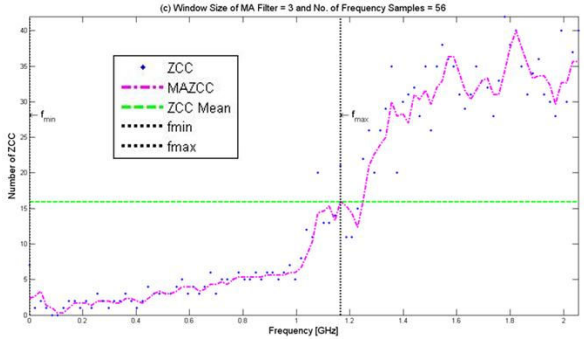

Figure 4: Moving average zero-crossing count vs frequency where the minimum frequency f_{min} = 21 MHz and the maximum frequency f_{max} = 1.19GHz.

3. Numerical results

The minimum and maximum frequencies are determined using the moving average zero-crossing count method (MAZCC) from Figure 4. Since the MAZCC does not cross the threshold at the lower frequency end, the lowest frequency (21 MHz) is selected as the minimum frequency. The MAZCC crosses the threshold at 1.19 GHz. This is chosen as the maximum frequency. When additive white Gaussian noise is added in the time-domain scattered field, the MAZCC method is also able to provide a suitable bandwidth as the magnitude observation method. When the signal-to-noise ratio, E_0/N is 20 dB, the minimum frequency and maximum frequencies are 127 MHz and 911 MHz respectively as shown in Figure 5.

Figures 6 and 7 show the DT inversion results obtained using the MAZCC method and the magnitude observation method respectively. The MAZCC method used the frequency range of 127 MHz – 911 MHz while the magnitude observation method used 64 MHz – 810 MHz. The two results are almost similar.

For a noisy scenario when E_0/N is 0 dB, the minimum and maximum frequencies are found to be 127 MHz and 700 MHz respectively as shown in Figure 8. Any frequency range broader than the MAZCC frequency range will lead to image distortion in the reconstruction buried object.

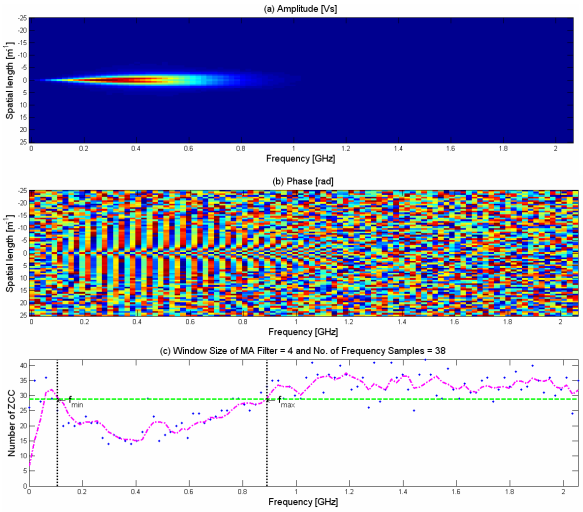

Figure 5: FT scattered field in spatial-frequency domain with E_0/N = 20 dB. (a) Spectral magnitude. (b) Spectral phase. (c) MAZCC method for frequency range selection

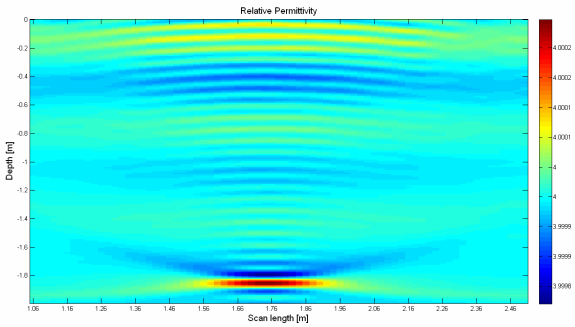

Figure 6: DT inversion result obtained from the MAZCC method (127 MHz – 911 MHz).

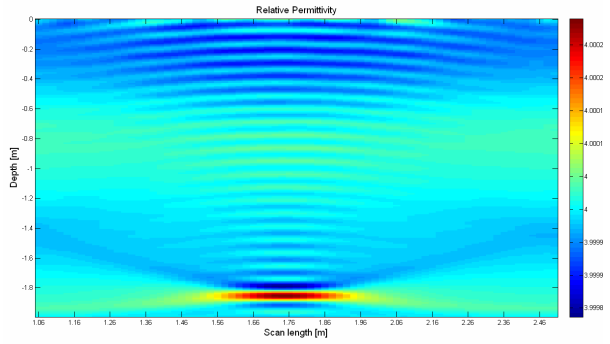

Figure 7: DT inversion result obtained from the magnitude observation method (64 MHz – 810 MHz).

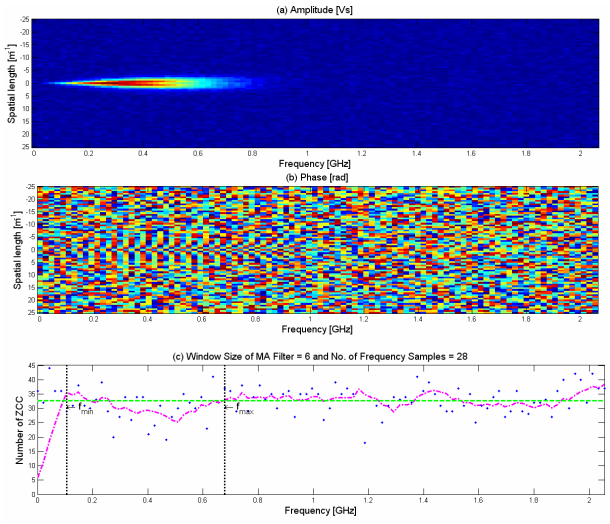

Figure 8: FT scattered field in spatial-frequency domain with E_0/N = 0 dB. (a) Spectral magnitude. (b) Spectral phase. (c) MAZCC method for frequency range selection

4. Conclusion

A maximum frequency range should be applied in a DT inversion routine to obtain a unique solution for the object function. We proposed an alternative bandwidth truncation method using the information on the phase variation of the 2D FT scattered field. From the numerical results, the moving average zero-crossing count method (MAZCC) can also give the suitable bandwidth compared with the magnitude observation method. The MAZCC method can be also applied to select the frequency range when the signal-to-noise ratio is small.

Acknowledgement

The authors would like to show gratitude to Dr. A. Giannopoulos, UK, for his generosity of sharing his GPRMax program which is an open sourced program and Dr. H. Thorkild, US, for helpful discussions on frequency range selection.

References

[1] D. Daniels, Ground Penetrating Radar, 2ed. London, U.K.: IEE Press, 2004.

[2] A. J. Devaney, "A computer simulation study of diffraction tomography," IEEE Transactions Biomedical Engineering, vol. GE-30, pp. 377-386, 1983.

[3] A. J. Devaney, "Geophysical diffraction tomography," IEEE Transactions Geoscience and Remote Sensing, vol. GE-22, pp. 3-13, 1984.

[4] J. C. Bolomey and C. Pichot, "Microwave tomography: From theory to practical imaging system," International Journal of Systems and Technology, vol 2, pp. 144-156, 1990

[5] T. J. Cui and W. C. Chew, "Novel diffraction tomographic algorithm for imaging two-dimensional targets buried under a lossy Earth," IEEE Transactions on Geoscience and Remote Sensing, vol. 38, pp. 2033-2041, 2000

[6] T. B. Hansen and P. M. Johansen, "Inversion scheme for ground penetrating radar that takes into account the planar air-soil interface," IEEE Transactions on Geoscience and Remote Sensing, vol. 38, pp. 496-506, 2000.

[7] T. J. Cui and W. C. Chew, "Diffraction tomographic algorithm for the detection of three-dimensional objects buried in a lossy half-space," IEEE Transactions on Antennas and Propagation, vol. 50, pp. 42-49, 2002

[8] G. Hislop and T. Tang, "A new diffraction tomography algorithm for ground penetrating radar," in Proceedings of the IEEE International Geoscience and Remote Sensing Symposium, IGARSS, 2003, pp. 4151-4153.

[9] C. K. Avinash and S. Malcolm, Principles of Computerized Tomographic Imaging, New York, USA: IEEE Press, 1988

[10] A. Giannopoulos, "Modelling ground penetrating radar by GprMax," Construction and Building Materials, vol. 19, no. 10m, pp. 755-762, 2005

[11] S. Smith, The Scientist and Engineer's Guide to Digital Signal Processing, California Technical Publishing, 1997.